Evolution of higher-order bright solitons in a nonlinear medium with memory

L. Gilles,* H. Bachiri, and L. Vázquez
Departamento de Matemática Aplicada, Escuela Superior de Informática, Universidad Complutense, E-28040 Madrid, Spain
(Received 10 November 1997)

Numerical integration of Maxwell's equations for propagation of a femtosecond pulse in a medium with memory characterized by linear and nonlinear Lorentz responses is carried out using the finite-difference time-domain method recently applied to the field of nonlinear optics. The main dynamical features, interference mechanisms of initial higher-order bright solitons under the combination of dispersion, self-phase modulation, and Raman self-scattering, are considered and compared to the case of an instantaneous nonlinear response. [S1063-651X(98)02905-5]

PACS number(s): 42.65.Ky

I. INTRODUCTION

Wave propagation in dispersive nonlinear media has attracted considerable attention in the past decade [1], in part motivated by its potential applications to optical fiber communication systems. Propagation of picosecond optical pulses in monomode optical fibers is governed by the nonlinear Schrödinger (NLS) equation describing the effects of group velocity dispersion (GVD) and the refractive index nonlinearity. Its general form is given by

$$i\left(\frac{\partial A}{\partial x}+\frac{1}{v_g}\frac{\partial A}{\partial t}\right)+i\frac{\Gamma_0}{2}A-\frac{1}{2}\beta_2\frac{\partial^2 A}{\partial t^2}+\sigma|A|^2A=0, \quad (1)$$

which can be simplified to

$$i\frac{\partial A}{\partial \xi}+i\frac{\Gamma_0}{2}A-\frac{1}{2}\beta_2\frac{\partial^2 A}{\partial \tau^2}+\sigma|A|^2A=0 \quad (2)$$

if time and space are measured in the group velocity frame $\tau=t-x/v_g$, $\xi=x$. The NLS equation is obtained directly from the governing Maxwell equations by a standard reductive perturbation procedure [2] within the slowly varying envelope approximation (SVEA), meaning that the pulse envelope $A(x,t)$ modulating the underlying carrier wave $\exp[i(k_0x-\omega_0t)]$ is assumed to be slowly varying in both time and space, which is expressed by the four conditions

$$\frac{\partial_x^2 A}{k_0\partial_x A}\sim O(\epsilon)\ll 1, \quad \frac{\partial_x A}{k_0 A}\sim O(\epsilon)\ll 1,$$

$$\frac{\partial_t^2 A}{\omega_0\partial_t A}\sim O(\epsilon)\ll 1, \quad \frac{\partial_t A}{\omega_0 A}\sim O(\epsilon)\ll 1. \quad (3)$$

Clearly, the SVEA imposes different requirements on the physical system. The ''local'' assumption of the SVEA (for a pulse traveling in the space direction) demands that the pulse width τ_{FWHM} must be much longer than the carrier oscillation period $T_0=2\pi\omega_0^{-1}$, i.e., the ratio of the spectral frequency width to the carrier frequency is a small parameter $\epsilon\sim O(\Delta\omega/\omega_0)\sim O(T_0/\tau_{\mathrm{FWHM}})\ll 1$ (quasimonochromatic approximation). The ''nonlocal'' part of the SVEA requires that the envelope must not significantly change as the pulse propagates over a distance equal to the carrier oscillation wavelength λ_0, which is reflected mathematically by the fact that the envelope equation contains only the first derivative with respect to the coordinate along the propagation direction, in contrast with Maxwell's wave equation, which is of second order in the propagation coordinate. Hence it can be solved with substantially less computational effort than Maxwell's wave equation. This benefit has been exploited in the investigation of a vast number of nonlinear optical phenomena [3]. Processes involving a backward propagating pulse violate the latter nonlocal contribution.

The progress of ultrashort laser optics [4] has now arrived at a point where light pulses with durations comparable to the carrier oscillation cycle have become available [5]. For subpicosecond optical pulse durations (width up to $\sim$ 50 fs), the NLS equation should be modified. The spectral width of such pulses becomes comparable to the carrier frequency and three main higher-order effects become important: (i) third-order dispersion (TOD), (ii) self-steepening (SS), and (iii) Raman self-scattering (RSS). TOD is a higher-order linear effect arising from the wavelength dependence of GVD, while SS and RSS are nonlinear processes resulting respectively from the intensity dependence of the group velocity (i.e., nonlinear dispersion) and the delayed response of the nonlinearity. Among the three higher-order physical effects, the intrapulse Raman stimulated scattering is the dominant perturbation and is among the most important nonlinear interactions that occur in optical fibers.

RSS produces a continuous downshift (redshift) of the soliton carrier frequency, a phenomenon know as soliton self-frequency shift [6], and, consequently, in the anomalous dispersion regime, a continuous deceleration of the pulse. Since its experimental discovery [7], numerical [8] and experimental [9] investigations of higher-order nonlinear effects resulting from the finite response time of the material nonlinearity have been carried out extensively because of their fundamental as well as technological importance. Raman induced optical shocks and kink solitons representing shock fronts propagating undistorted inside optical fibers have been predicted [10]. Carrier wave shocking of femtosecond optical pulses as a result of a SS effect producing two

*Electronic address: fite1z2@sis.ucm.es

well-separated events, one on the optical carrier and the other on the envelope of the carrier, has been evidenced [11]. The conditions for complete compensation of the soliton self-frequency shift by a proper choice of the optical gain spectrum and the dispersion parameters of the media have been given [12]. Phase-sensitive amplifiers have been demonstrated in this context to act as a restoring force in frequency, constraining the pulse to remain near its carrier wavelength [13]. Soliton interactions induced by higher-order nonlinear effects have also received a great deal of attention with the advances in soliton laser technology [14], mainly because of their key role in the propagation of an ultrahigh bit rate coherent soliton train through optical fibers [15]. Migration of the intersoliton phase difference associated with RSS forces the solitons carrying the information bits into a deleterious attractive phase relationship, which is detrimental to the bit-error rate. Therefore, the effects of various influences on the propagation of solitons including periodic amplification, higher-order dispersion, and Raman scattering losses, each of which will be increasingly important for shorter pulse widths, have to be well understood. The goal of the present contribution is to address and analyze among these influences the important ultrafast nonlinear process of Raman scattering.

Different generalized versions of the nonlinear Schrödinger equation have been proposed to model the former higher-order processes. Following the perturbative Kodama- and Hasegawa (KH) approach [16], a generalized nonlinear Schrödinger (GNLS) equation including three additional terms representing the dominant higher-order effects is suggested. Including the higher-order terms, the KH GNLS equation may be written as

$$i\frac{\partial A}{\partial \xi}+i\frac{\Gamma_0}{2}A-\frac{1}{2}\beta_2\frac{\partial^2 A}{\partial \tau^2}+\sigma|A|^2A+h=0, \tag{4}$$

where h represents the higher-order effects

$$h=i\left(-\frac{\beta_3}{6}\frac{\partial^3 A}{\partial \tau^3}+\sigma_1\frac{\partial}{\partial \tau}(|A|^2A)+\sigma_2 A\frac{\partial |A|^2}{\partial \tau}\right). \tag{5}$$

The three higher-order terms describe respectively TOD, SS, and RSS. The KH GNLS equation correctly describes the higher-order nonlinear effects for optical pulses as short as $\sim$50 fs [full width at half maximum (FWHM)]. For much shorter pulses, it fails to provide a correct physical description since the effects of Raman gain are included only to first order. A more exact one-dimensional (1D) integro-differential envelope equation has been derived [17] by Blow and Wood and should be used in that case for a correct description of SRS. The Blow-Wood (BW) GNLS equation expressed by

$$i\frac{\partial A}{\partial \xi}+i\frac{\Gamma_0}{2}A-\frac{1}{2}\beta_2\frac{\partial^2 A}{\partial \tau^2}-i\frac{\beta_3}{6}\frac{\partial^3 A}{\partial \tau^3}+\sigma\left(1+\frac{i}{\omega_0}\frac{\partial}{\partial \tau}\right)\times\left[A\int_{-\infty}^{\tau}R(\tau-\tau_1)|A(\xi,\tau_1)|^2d\tau_1\right]=0 \tag{6}$$

yields the KH GNLS equation under the assumption of short delays. The BW formalism does not rely directly on the SVEA; it only assumes that there are at least three optical cycles within the envelope, i.e., $\epsilon\leqslant 1/3$, and neglects backward propagating waves. Recently, a general 3D wave equation first order in the propagation coordinate was suggested by Brabec and Krausz [18] and the concept of envelope equations was shown to be applicable to the single-cycle regime of nonlinear optics. In the frame of the Brabec-Krausz GNLS equation, not only the envelope but also the carrier *phase* must not vary significantly as the pulse covers a distance equal to the carrier wavelength [the so-called slowly evolving wave approximation (SEWA)]. On the other hand, it does not impose a limitation on the pulse width.

In this paper, we solve directly the 1D Maxwell equations for the evolution of an initial sub-(50-fs)multisoliton pulse in a nonlinear medium with memory in both the linear and nonlinear polarizations. For illustrative purposes we have chosen an initial third-order bright soliton pulse of duration equal to 25.7 fs (FWHM) containing eight carrier oscillation cycles. The finite-difference (FD) time-domain (TD) method, proposed recently as a computational tool for the field of nonlinear optics [19], discretizes the differential form of Maxwell's partial differential equations (PDEs) appended by a set of ordinary differential equations (ODEs) for the memory integrals and provides an accurate description of the pulse evolution for the given constitutive relation between the electric field and polarizations, without recourse to the SVEA or SEWA. We restrict our attention to nonmagnetic Kerr media with no free charges. We examine dynamical multisoliton pulse breathing mechanisms before and after the ''foci'' point, the decay and formation of fundamental solitons under the influence of the higher-order nonlinear effects. A systematic comparison with a dielectric medium characterized by an instantaneous nonlinear response is performed throughout.

II. GOVERNING EQUATIONS

We consider the time-dependent evolution of a one-dimensional pulse of right circular polarization in the y-z plane, traveling along the x axis. Maxwell's equations for the electric- and magnetic-field quantities **E,H** are

$$\nabla\times\mathbf{E}=-\mu_0\partial\mathbf{H}/\partial t,$$

$$\nabla\times\mathbf{H}=\partial\mathbf{D}/\partial t. \tag{7}$$

The material linear and nonlinear responses are included through the constitutive relation $\mathbf{D}=\epsilon_0[\mathbf{E}+\mathbf{\Phi}]$, where $\mathbf{\Phi}=\mathbf{\Phi}^{(1)}+\mathbf{\Phi}^{(3)}$ is the total induced electric macroscopic polarization, consisting of linear and nonlinear parts. If the time scale over which the medium changes (defined by the medium polarization) is of the order of the pulse duration, the effects of a finite response time must be taken into account. Mathematically, the memory effects are described through the convolution integrals

$$\mathbf{\Phi}^{(1)}(t)=\int_{-\infty}^{t}\chi^{(1)}(t-t_1)\mathbf{E}(t_1)dt_1, \tag{8}$$

$$\mathbf{\Phi}^{(3)}(t)=\int_{-\infty}^{t}\chi^{(3)}(t-t_1,t-t_2,t-t_3)\cdot\mathbf{E}(t_1)\mathbf{E}(t_2)\mathbf{E}(t_3)dt_1dt_2dt_3$$
$$=\int_{-\infty}^{t}\Delta\chi^{(3)}(t-t_1)\mathbf{E}(t_1)dt_1,$$

$$\Delta\chi^{(3)}(t-t_1)=\int_{-\infty}^{t}\chi^{(3)}(t-t_1,t-t_2,t-t_3)\cdot\mathbf{E}(t_2)\mathbf{E}(t_3)dt_2dt_3. \quad (9)$$

For simplicity, a centrosymmetric and isotropic material has been assumed, so that the second-order susceptibility tensor $\chi^{(2)}$ is identically zero, $\chi^{(1)}=\chi^{(1)}_{yy}=\chi^{(1)}_{zz}$ and $\chi^{(3)}=\chi^{(3)}_{yyyy}=\chi^{(3)}_{zzzz}$ [20]. As a consequence of isotropy, the electric induction field **D** and the electric field **E** are parallel. Third-order nonlinear effects include the quadratic electro-optic (dc Kerr) effect, third-harmonic generation, four-wave mixing, intensity-dependent refractive index, stimulated Raman and Brillouin scattering, and two-photon absorption. The physical mechanisms contributing to the nonlinear third-order electric susceptibility far from electronic absorption (i.e., in the visible or infrared spectral regions because the electronic absorption lies in the ultraviolet) are of two different types and contribute additively to $\chi^{(3)}$ [21]. An ''electronic'' contribution, nearly instantaneous ($\sim$ 0.1 fs), arises from the electronic response to the applied electric field against the heavy nuclei considered fixed at an average position. The second ''nuclear'' contribution arises from the electric-field-induced changes in the internal nuclear vibrations on a much longer time scale ($\sim$ 100 fs) and are usually temperature dependent. To model in a classical electrodynamical picture these interactions [22,23], the cubic polarization must be proportional to the electric field at time t times a convolution of the field intensity at earlier times (related to the intensity-dependent small displacement of the vibrating nuclei from equilibrium). Equation (9) is then simplified to

$$\mathbf{\Phi}^{(3)}(t)=\Delta\chi^{(3)}(t)\mathbf{E}(t),$$

$$\Delta\chi^{(3)}(t)=\int_{-\infty}^{t}\chi^{(3)}(t-t_1)\|\mathbf{E}(t_1)\|^2dt_1,$$

$$\chi^{(3)}(t)=a[(1-\theta)\delta(t)+\theta g_v(t)], \quad (10)$$

where a is the nonlinear coupling constant and θ parametrizes the relative strength of the instantaneous and delayed interactions. Thus the third-order memory function $\Delta\chi^{(3)}$ is expressed as the sum of electronic instantaneous and molecular vibrational delayed parts

$$\Delta\chi^{(3)}=\Delta\chi^{(3)}_{\mathrm{Kerr}}+\Delta\chi^{(3)}_{v},$$

$$\Delta\chi^{(3)}_{\mathrm{Kerr}}=a(1-\theta)\|\mathbf{E}\|^2,$$

$$\Delta\chi^{(3)}_{v}=a\theta\mathcal{Q}_v. \quad (11)$$

$\mathcal{Q}_v$ describes the natural oscillation within the dielectric material with frequency many orders of magnitude less than the optical wave frequency, responding to the field intensity. Later, we will see that $\mathcal{Q}_v$ can be thought of as being the normal mode amplitude of a driven damped harmonic oscillator. In general, the nonlinear susceptibility $\chi^{(3)}$ will differ from $\chi^{(1)}$ in physical properties such as resonances and relaxations. In terms of the Fourier transform

$$\mathbf{E}(t)=\frac{1}{2\pi}\int_{-\infty}^{\infty}\hat{\mathbf{E}}(\omega)\exp(i\omega t)d\omega,$$

$$\hat{\mathbf{E}}(\omega)=\int_{-\infty}^{\infty}\mathbf{E}(t)\exp(-i\omega t)dt, \quad (12)$$

the medium polarizations are written as

$$\hat{\mathbf{\Phi}}^{(1)}(\omega)=\hat{\chi}^{(1)}(\omega)\hat{\mathbf{E}}(\omega),$$

$$\hat{\mathbf{\Phi}}^{(3)}(\omega)=\int_{-\infty}^{\infty}\Delta\hat{\chi}^{(3)}(\omega_v)\hat{\mathbf{E}}(\omega-\omega_v)d\omega_v,$$

$$\Delta\hat{\chi}^{(3)}(\omega_v)=\hat{\chi}^{(3)}(\omega_v)\int_{-\infty}^{\infty}\hat{\mathbf{E}}(\Omega)\hat{\mathbf{E}}^{*}(\Omega-\omega_v)d\Omega. \quad (13)$$

From Eq. (13) the three-wave interaction process can be regarded as the scattering of the spectral component $\hat{\mathbf{E}}(\omega-\omega_v)$ into the third-order polarization wave spectral component $\hat{\mathbf{\Phi}}^{(3)}(\omega)$ and nuclear vibrations $\Delta\hat{\chi}^{(3)}(\omega_v)$, which in turn are excited by every pair of spectral components separated by ω_v. Because of causality [i.e., the susceptibility functions $\chi^{(1)}(t)$ and $\chi^{(3)}(t)$ are zero for $t<0$], the Fourier transforms $\hat{\chi}^{(1)}(\omega),\hat{\chi}^{(3)}(\omega)$ exist and are differentiable for all real ω only if the real variable ω is extended into the upper complex plane $\omega=\omega_r+i\omega_i$ with $\omega_i>0$ (strictly positive), yielding the Kramers-Krönig relations between the real and imaginary parts of each Fourier transform and ensuring $\int_{-\infty}^{\infty}|\chi^{(1)}(t)|dt<\infty$ and $\int_{-\infty}^{\infty}|\chi^{(3)}(t)|dt<\infty$. Note that since the susceptibility functions are real, the real part of their Fourier transform is symmetric and the imaginary part antisymmetric.

To establish the link between the susceptibility formalism and the description of dynamic nonlinear optical processes it is useful to introduce the important concept of optical field induced refractive index. For simplicity, we restrict our attention to right circularly polarized fields, i.e., $\mathbf{E}=[0,E_y,E_z]^T$, and $\mathbf{H}=[0,H_y,H_z]^T$, represented by

$$\mathbf{E}(x,t)=\frac{1}{2}\mathbf{q}(x,t)\exp[i(k_0x-\omega_0t)]+\text{c.c.},$$

$$\mathbf{H}(x,t)=\frac{1}{2}\mathbf{h}(x,t)\exp[i(k_0x-\omega_0t-\pi/2)]+\text{c.c.}, \quad (14)$$

which satisfy the phase relations $q_z=-iq_y$ and $h_z=-ih_y$, in which case new complex scalar wave packets can be defined as

$$\begin{bmatrix}E(x,t)\\H(x,t)\\D(x,t)\end{bmatrix}=\begin{bmatrix}q(x,t)\\h(x,t)\\d(x,t)\end{bmatrix}\exp[i(k_0x-\omega_0t)], \quad (15)$$

where $E=E_y+iE_z$, $H=iH_y-H_z$, and $D=D_y+iD_z$ and for which the third-harmonic polarization is absent since $\|\mathbf{E}\|^2=|E|^2=|q(x,t)|^2$. The corresponding Maxwell equations are written as

$$\frac{\partial}{\partial t}H=\frac{1}{\mu_0}\frac{\partial}{\partial x}E,$$

$$\frac{\partial}{\partial t}D=\frac{\partial}{\partial x}H,$$

$$D=\epsilon_0[E+\Phi^{(1)}+\Phi^{(3)}], \tag{16}$$

or in the form of a wave equation for the complex E field

$$\frac{\partial^2}{\partial t^2}E-c^2\frac{\partial^2}{\partial x^2}E+\frac{\partial^2}{\partial t^2}\Phi=0. \tag{17}$$

In frequency space, assuming that $\hat{\Phi}^{(3)}\sim\Delta\hat{\chi}^{(3)}(\omega)\hat{E}(\omega)\sim\hat{\chi}^{(3)}(\omega)|E|^2$, the wave equation reads

$$\frac{\partial^2}{\partial x^2}\hat{E}+\epsilon(\omega)\frac{\omega^2}{c^2}\hat{E}=0, \tag{18}$$

where

$$\epsilon(\omega)=1+\hat{\chi}^{(1)}(\omega)+\Delta\hat{\chi}^{(3)}(\omega) \tag{19}$$

is the dielectric function whose third-order contribution $\Delta\hat{\chi}^{(3)}(\omega)$ is proportional to the field intensity. Since $\hat{\chi}^{(1)}(\omega)$ and $\hat{\chi}^{(3)}(\omega)$ are in general complex, so is the dielectric function $\epsilon(\omega)$. Its real and imaginary parts are related to the refractive index $n(\omega)$ and the absorption loss coefficient $\Gamma(\omega)$ through the relationship

$$\epsilon(\omega)=\left[n(\omega)+i\Gamma(\omega)\frac{c}{2\omega}\right]^2. \tag{20}$$

Therefore,

$$n(\omega)=n_0(\omega)+n_2|E|^2,$$

$$\Gamma(\omega)=\Gamma_0(\omega)+\Gamma_2(\omega)|E|^2, \tag{21}$$

where the linear and nonlinear optical induced refractive indices are given by

$$n_0(\omega)=\mathrm{Re}[\sqrt{1+\hat{\chi}^{(1)}(\omega)}],$$

$$n_2\sim\frac{\hat{\chi}^{(3)}(0)}{2n_0(\omega_0)}\sim\frac{a[(1-\theta)+\theta\hat{g}_v(0)]}{2n_0(\omega_0)}, \tag{22}$$

while the single- and two-photon absorption coefficients are

$$\Gamma_0(\omega)=\frac{\omega_0}{n_0(\omega_0)c}\mathrm{Im}[\hat{\chi}^{(1)}(\omega)],$$

$$\Gamma_2(\omega)=\frac{\omega_0}{n_0(\omega_0)c}\mathrm{Im}[\hat{\chi}^{(3)}(\omega)]=\frac{a\theta\omega_0}{n_0(\omega_0)c}\mathrm{Im}[g_v(\omega)]. \tag{23}$$

To a good approximation for the visible and infrared spectral regions, the frequency dependence of the nonlinear refractive index is not important and dominated by the Kerr nonlinearity. The fraction θ of the nonlinear index coming from the delayed nonlinear response can be obtained from measurable values of n_2 [24]. The imaginary part of the third-order susceptibily Γ_2 describes the Raman gain profile, responsible for the RSS process. The continuous spectrum of the gain profile stretches from zero up to $\sim 440\ \mathrm{cm}^{-1}$ (~ 13 THz), which covers the broad spectrum of femtosecond optical soliton pulses. The Raman gain can then amplify the low-frequency (Stokes) components of ultrashort wave packets by pumping energy from their high-frequency (anti-Stokes) components. Consequently, the center frequency of the pulse continuously decreases during propagation (soliton self-frequency shift) [6].

Recently, a different approach in the nonlinear optics community, emerging from the FD TD solution of Maxwell's equations, has been shown to be particularly well suited to model electromagnetic nonlinear phenomena inside compact optical devices such as optical fibers, couplers, switches, and amplifiers [19]. Within this framework, the medium memory (i.e., the linear and nonlinear dispersive properties) is described by a set of ODEs appended to Maxwell's PDEs (16). The ODEs represent the dynamic equations of the convolution integrals $\Phi^{(1)}$ and $\mathcal{Q}_v$ driven by the electric field and its intensity, respectively. Here we model the kernel functions by Lorentz linear dipole oscillators of single resonance frequency,

$$\hat{\chi}^{(1)}(\omega)=\frac{\beta_1\omega_1^2}{\omega_1^2+2i\gamma\omega-\omega^2},$$

$$\hat{g}_v(\omega)=\frac{\Omega_v^2}{\Omega_v^2+2i\gamma_v\omega-\omega^2}, \tag{24}$$

where ω_1, γ, Ω_v, and γ_v characterize the resonance frequency and bandwidth of the linear dipole oscillators modeling the medium response. In the time domain, the kernel functions obey damped harmonic-oscillator equations of motion

$$\ddot{\chi}^{(1)}(t)+2\gamma\dot{\chi}^{(1)}(t)+\omega_1^2\chi^{(1)}=0,$$

$$\ddot{g}_v+2\gamma_v\dot{g}_v+\Omega_v^2 g_v=0, \tag{25}$$

whose solutions take the forms

$$\chi^{(1)}(t)=\frac{\beta_1\omega_1^2}{\nu_0}\exp(-\gamma t)\sin(\nu_0 t)\Theta(t),$$

$$g_v(t)=\frac{\Omega_v^2}{\nu_v}\exp(-\gamma_v t)\sin(\nu_v t)\Theta(t), \tag{26}$$

where $\nu_0=\sqrt{\omega_1^2-\gamma^2}$ and $\nu_v=\sqrt{\Omega_v^2-\gamma_v^2}$. This property of the kernel functions allows one to treat the memory integrals $\Phi^{(1)},\mathcal{Q}_v$ as new dependent variables governed by driven damped Lorentz oscillator equations

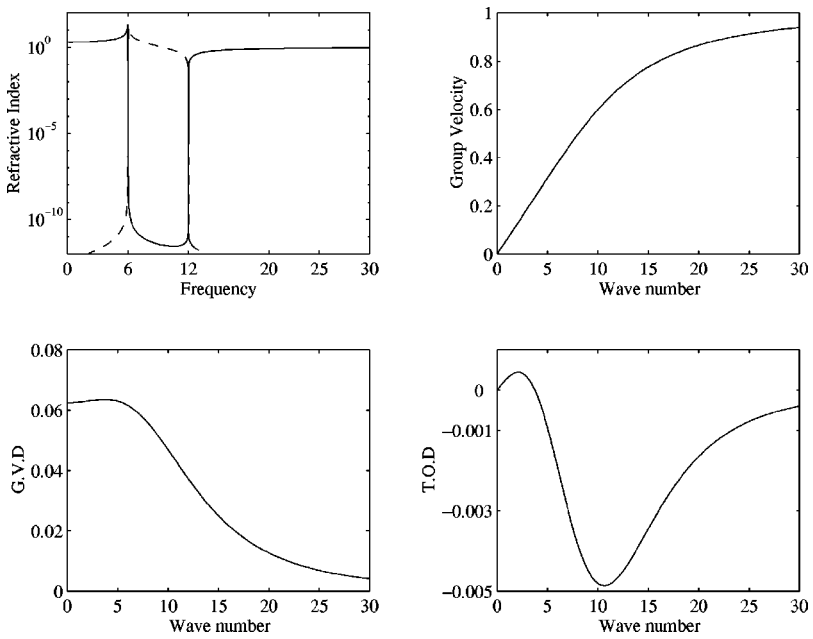

FIG. 1. Theoretical linear chromatic dispersion features: linear refractive index (solid curve) and absorption coefficient (dashed curve), group velocity, group velocity dispersion, and third-order dispersion for a Lorentz medium characterized by a single resonance frequency $\omega_1 t_0 = 6$, static relative permittivity equal to $1+\beta_1 = 4$, and damping rate equal to $\gamma t_0 = 10^{-9}$.

$$\ddot{\Phi}^{(1)} + 2\gamma\dot{\Phi}^{(1)} + \omega_1^2\Phi = \beta_1\omega_1^2 E,$$

$$\ddot{\mathcal{Q}}_v + 2\gamma_v\dot{\mathcal{Q}}_v + \Omega_v^2\mathcal{Q}_v = \Omega_v^2|E|^2. \tag{27}$$

Such a phenomenological description of the interaction between light and matter relies on the Born-Oppenheimer approximation. The ODEs (27) are coupled simultaneously to Maxwell's PDEs (16) and numerically integrated in a moving coordinate system in order to keep the pulse slowly moving on the computational grid, using a second-order-in-time, second-order-in-space nonlinear FD TD method with radiation boundary conditions describing the outgoing field behavior. A detailed stability and phase error analysis of FD TD methods in dispersive media has been carried out recently [25] and our discretization has been chosen accordingly. In the absence of memory in the material nonlinearity, the resulting system is of the Hamiltonian type since intrinsic to RSS is a nonlinear absorption effect by nuclear vibations. We have analyzed elsewhere [26] an energy-conserving FD TD scheme for Maxwell's equations including the instantaneous Kerr nonlinearity.

III. EVOLUTION OF HIGHER-ORDER BRIGHT SOLITONS

Since the influence of RSS strongly depends on the peak intensity and spectral width of the pulse, we expect the Raman effect to affect significantly the evolution properties of initial higher-order solitons known to have an important narrowing during the initial stage of evolution [27]. As an illustrative example we have chosen an initial hyperbolic secant third-order bright soliton pulse of duration equal to 25.7 fs (FWHM) (time constant $t_0 = 14.6$ fs and $ct_0 = 4.38$ μm) centered at $\lambda_0 = 0.96$ μm (vacuum wavelength of 0.9 μm):

$$E(x, t=0) = NE_0\ \mathrm{sech}(x/ct_0)\exp(2i\pi/\lambda_0), \tag{28}$$

with $N=3$. The dimensionless carrier wave number and frequency are equal to $k_0 ct_0 = 28.56$ and $\omega_0 t_0 = 30.46$, respectively. The peak intensity of the initial E field is equal to $N^2E_0^2$ and its full width at half maximum ($1.76ct_0 = 7.71$ μm) contains eight carrier oscillation wavelengths. Approximate initial values for H and D can be obtained from the Fourier transform of Eqs. (16) and (27) [26]. Figure 1 shows typical theoretical material chromatic dispersion features in the optical range, obtained from the expression for $\hat{\chi}^{(1)}(\omega)$.

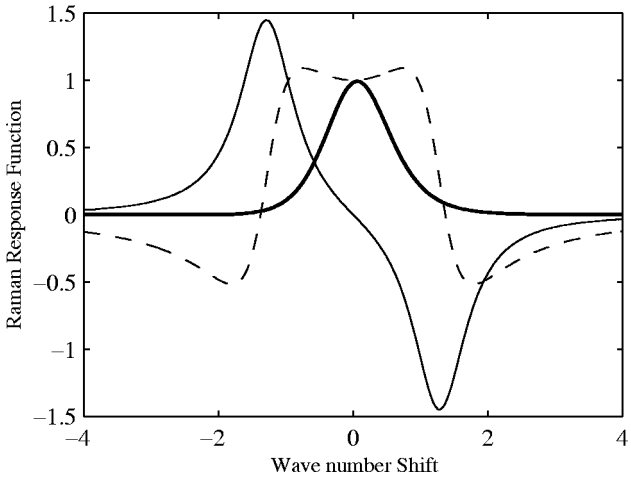

FIG. 2. Theoretical Raman gain spectrum, real part of the Raman suceptibility (dashed curve), and intensity spectrum of the initial third-order soliton pulse (thick solid curve). The controlling parameters of the Raman model are $\nu_v t_0 \sim 1.2$ and $\gamma_v t_0 \sim 0.456$ ($\Omega_v t_0 = 1.28$). The initial soliton duration is equal to 25.7 fs (FWHM) (time constant $t_0 = 14.6$ fs and $ct_0 = 4.38$ μm) and is centered at $\lambda_0 = 0.96$ μm ($k_0 ct_0 = 28.56$ and vacuum wavelength of 0.9 μm).

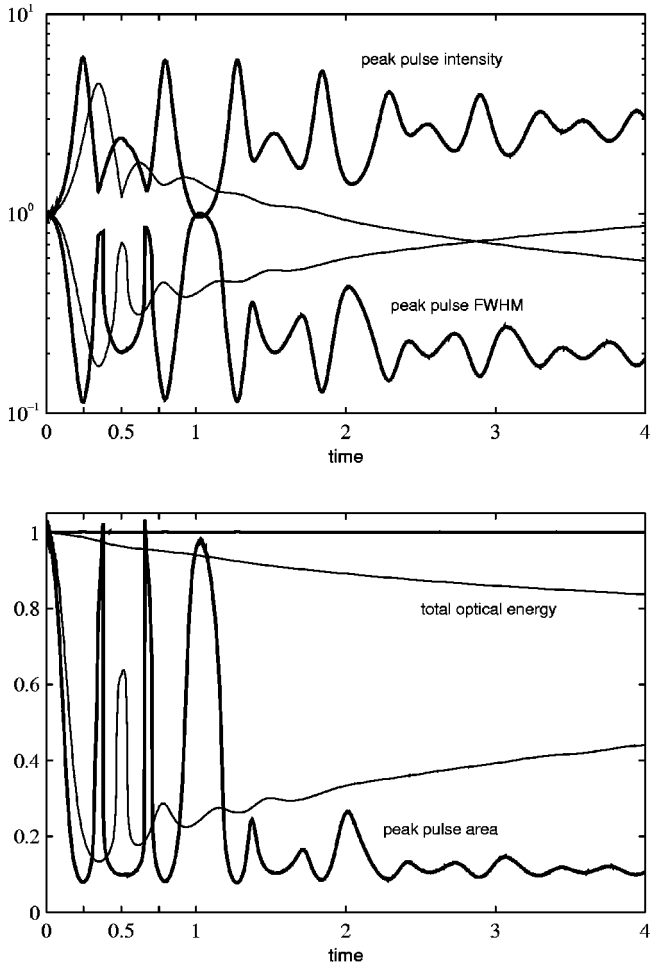

FIG. 3. Temporal dynamical evolution of the initial third-order soliton shown in Fig. 2 in the nonlinear dispersive Lorentz medium. Thick traces referring to the instantaneous Kerr model (nonlinear strength $aE_0^2=3\times10^{-4}$) are compared to the Raman model characterized by $\theta=0.3$ and Raman gain parameters are as given in Fig. 2.

The controlling parameters of the Lorentzian were assumed to be $\beta_1=3$ (static permittivity equal to $1+\beta_1$), $2\pi\omega_1^{-1}=15.3$ fs, ($\omega_1 t_0=6$), and $\gamma^{-1}=14.6$ μs ($\gamma t_0=10^{-9}$).

The long relaxation time (small damping) of the resonance causes two deep jumps of the linear refractive index at $\omega\sim\omega_1\sqrt{1+\beta_1}$ and $\omega\sim\omega_1$, which outside this absorption band increases slowly with frequency towards its infinite frequency value of unity. The zero dispersion point lies at infinity and the Lorentz medium exhibits anomalous dispersion ($\omega''>0$) over the spectral domain above the absorption band. The theoretical Raman gain profile is shown in Fig. 2 as a function of the dimensionless wave-number shift $(k-k_0)ct_0$, together with the real part of the Raman nuclear susceptibility and the intensity spectrum of the initial electric field whose FWHM in k space is equal to $1.12ct_0\sim4.9$ μm. The parameters defining the Raman Lorentz model are [17]: $\nu_v^{-1}=12.2$ fs, and $\gamma_v^{-1}=32$ fs ($\nu_v t_0\sim1.2$, and $\gamma_v t_0\sim0.456$) ($\Omega_v t_0=1.28$). The largest gain occurs at a wave number shifted downward by about $n_0\Omega_v t_0\sim1.23$ corresponding to 447 cm^{-1} (13.2 THz), which is of the order of the initial soliton spectral width. The initial peak intensity $q_0=NE_0$ and pulse width t_0 have been adjusted according to the NLS equation to exhibit solitonlike behavior from the balance between the second-order and nonlinear length scales

$$T_d^{(2)}=\frac{(ct_0)^2}{\omega''},$$

$$T_{\mathrm{Kerr}}=\frac{2c^2k_0}{\omega_0^2\omega' aq_0^2} \tag{29}$$

and the balance equation reads $N^2=T_d^{(2)}/T_{\mathrm{Kerr}}$, i.e.,

$$aE_0^2=\frac{2k_0\omega''}{\omega_0^2\omega' t_0^2}, \tag{30}$$

yielding the value $aE_0^2=310^{-4}$ for the chosen carrier wavelength.

For $N=3$, the initial pulse represents a third-order soliton, i.e., a bound state of three solitons characterized by three purely imaginary eigenvalues (controlling the soliton amplitude) of the eigenvalue problem associated with the inverse-scattering transformation (IST) in the context of the NLS equation [27]. The real part of the eigenvalues, characterizing the relative speed of the constitutive solitons, is zero in the absence of perturbations and the envelope of the higher-

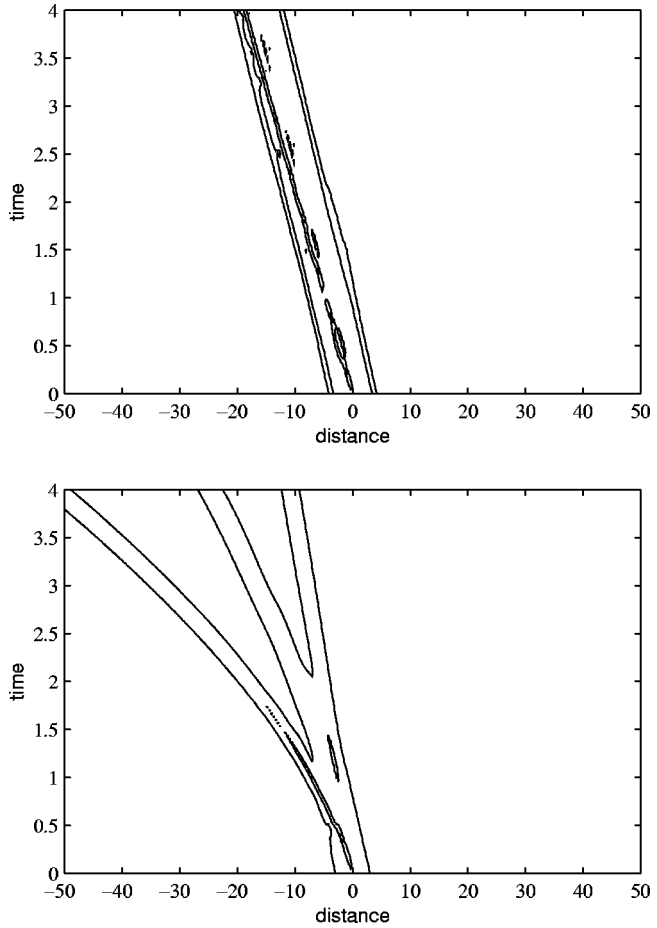

FIG. 4. Contour plots of the electric-field profile. The top picture is for the Kerr model ($\theta=0$) and the bottom picture is for the Raman model ($\theta=0.3$).

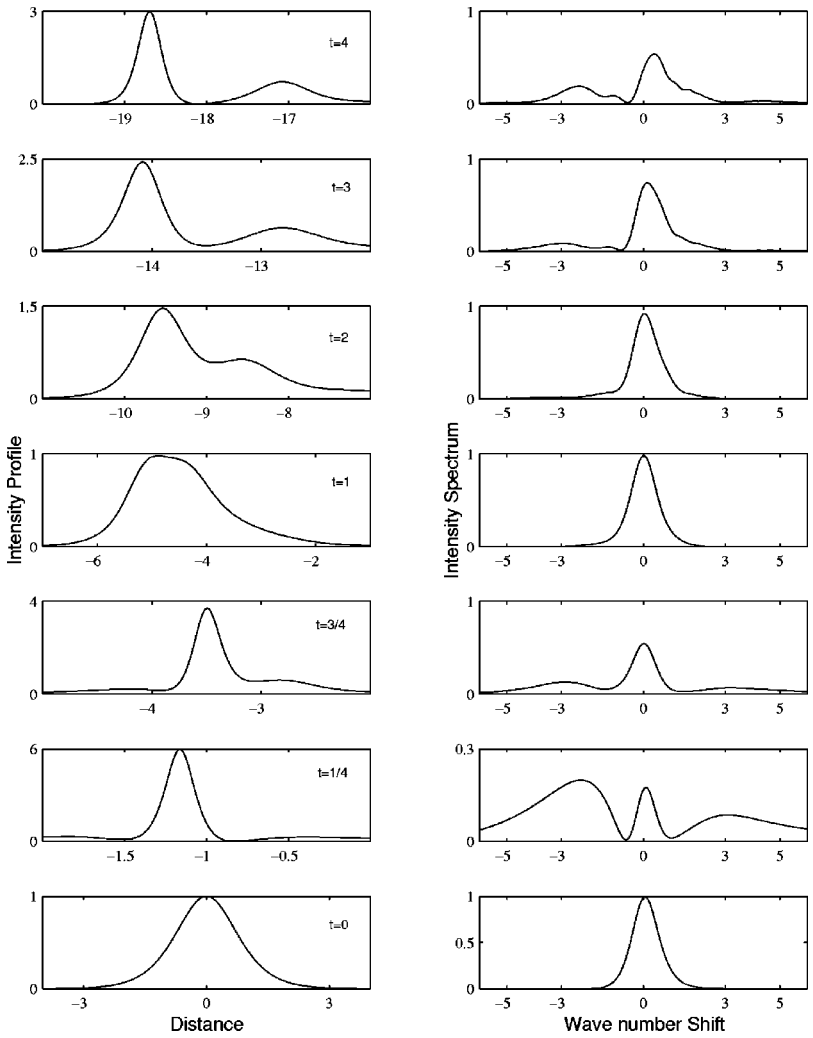

FIG. 5. Spatial and spectral dynamics of the decay of the third-order soliton caused by TOD and SS ($\theta=0$).

order soliton pulsates with period $(\pi/2)T_d^{(2)}\sim 336t_0$ due to phase interference among the constitutive solitons. The effect of higher-order dispersion (the joint effect of TOD and SS, or SS solely) is to modify the soliton velocity by an amount depending on its parameters (real and imaginary parts of the eigenvalues), leading, therefore, to the splitting of higher-order solitons into their constitutive fundamental components [16]. In the presence of a delayed medium nonlinearity, the soliton shifts to longer wavelengths through RSS within the bandwidth of the pulse and hence experiences a constant deceleration (see Fig. 1). The effect dominates over SS since the deviation in the velocity increases proportionally to the propagation distance. The differential frequency (or velocity) shift (i.e., deceleration) produced by RSS is, in the linear approximation, proportional to the slope of the Raman gain profile near $k=k_0$, $\partial_{\Delta k}\hat{g}_v(0)$, and to the inverse of the fourth power of the pulse width, t_0^{-4}, or E_0^4 [6]. Since the frequency shift depends on the amplitude, the most intense soliton decelerates more than the low-power one. Therefore, if the initial pulse contains solitons with different amplitudes (like a bound higher-order soliton), it will split into individual solitons with different amplitudes and velocities. The difference in the frequency shifts between solitons and their relative velocities is the key mechanism in the soliton splitting produced by the Raman delayed nonlinear response. Figure 3 shows the results of the numerical integration of Maxwell's equations for the initial $N=3$ soliton evolving over four soliton periods. We have chosen the value $\theta=0.3$ to parametrize the relative strength of the Kerr and Raman interactions. Thick traces correspond to the case of an instantaneous Kerr nonlinear response ($\theta=0$). To characterize solitonlike propagation regime, a useful parameter is given by the product of the peak pulse intensity and the square of its FWHM. For fundamental solitons, this measure of the ''pulse area'' is constant. The top picture displaying the peak pulse intensity and FWHM shows that in the absence of RSS the pulsating pattern of the initial three-solitons slowly decays, a signature of the splitting of the initial pulse into its component solitons and radiation, due to TOD and SS. The asymptotic height of each soliton is roughly $2\lambda_I/N=5/3,1,1/3$, where λ_I are the imaginary eigenvalues obtained from the IST. In contrast, RSS drastically changes the dynamical behavior of the propagating soliton. As a consequence of RSS, the wavelength and consequently the group velocity dispersion (see Fig. 1) continuously increase. However, since the energy of the soliton pulse (30) cannot increase, the soliton is forced to increase its width, which in turn decreases the differential frequency shift, since the latter is inversely proportional to the fourth power of the pulse width. From Fig. 3 we see that the Raman scattering clearly

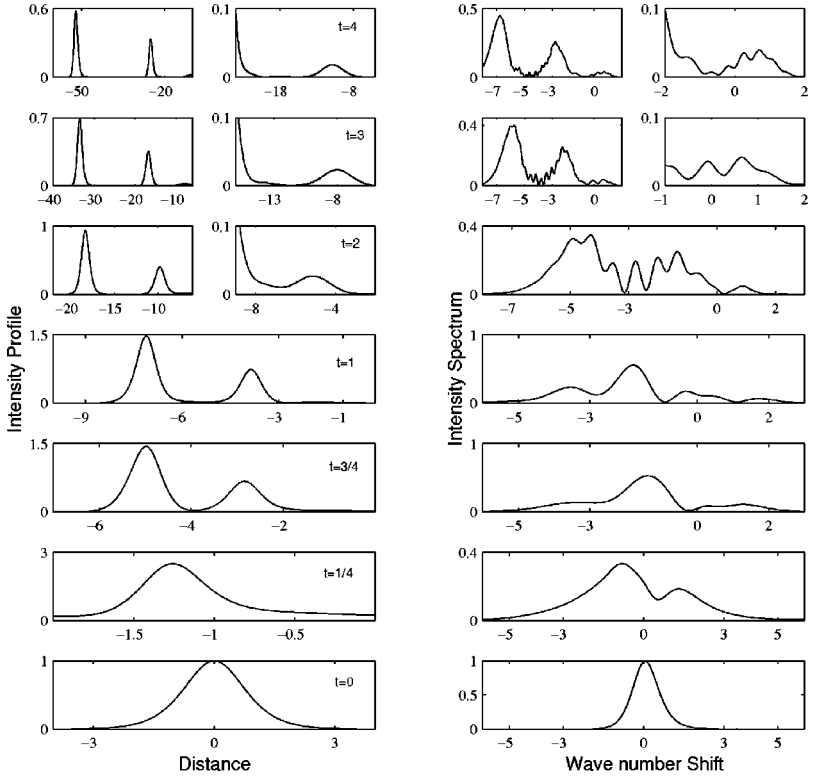

FIG. 6. Spatial and spectral dynamics of the decay of the initial third-order soliton due to RSS ($\theta=0.3$).

dominates the higher-order dispersive effects (TOD and SS). The initial stage of pulse compression is similar for both Kerr and Raman models, except that the point of maximum narrowing (foci) is delayed in the case of delayed nonlinearity, reflecting the fact that the spectral center of gravity has been downshifted to the Stokes side. The total normalized electromagnetic energy density calculated from Maxwell's PDEs (16) coupled to the ODEs (27) is defined as

$$\mathcal{E}(t)=\mathcal{E}_0+\mathcal{E}_{\Phi^{(1)}}+\mathcal{E}_{\mathcal{Q}_v}+\mathcal{E}_{\mathrm{NL}}, \tag{31}$$

where

$$\mathcal{E}_0=|H|^2+|E|^2,$$

$$\mathcal{E}_{\Phi^{(1)}}=\frac{|\dot{\Phi}^{(1)}|^2+\omega_1^2|\Phi^{(1)}|^2}{\beta_1\omega_1^2},$$

$$\mathcal{E}_{\mathcal{Q}_v}=\frac{a\theta}{2\Omega_v^2}[(\dot{\mathcal{Q}}_v)^2+\Omega_v^2\mathcal{Q}_v^2],$$

$$\mathcal{E}_{\mathrm{NL}}=a|E|^2\left[\frac{3}{2}(1-\theta)|E|^2+\theta\mathcal{Q}_v\right] \tag{32}$$

represent, respectively, the free-energy density and the harmonic and nonlinear contributions. The evolution equation for the energy density reads

$$\frac{\partial}{\partial t}\mathcal{E}=-\frac{4\gamma|\dot{\Phi}^{(1)}|^2}{\beta_1\omega_1^2}-\frac{a\theta\gamma_v(\dot{\mathcal{Q}}_v)^2}{\Omega_v^2}. \tag{33}$$

The two terms on the right-hand side of Eq. (33) describe, respectively, the linear (single-photon) and nonlinear (two-photon) absorption losses, clearly illustrated in Fig. 3.

In Fig. 4 we present contour plots of the electric field. The top picture, for the Kerr model, indicates a slight separation of the most intense part of the pulse that is delayed due to higher-order dispersion. The distance is measured in the group velocity frame $x'=(x-vt)/ct_0$ (the leading edge of the initial pulse lies at $x'>0$). The bottom picture, for the Raman model, shows clearly the constant deceleration of the Stokes downshifted pulse and splitting of the initial bound three-soliton state.

Finally, we show snapshots of the spatial and spectral pulse intensity profile at different characteristic times $t=0,1/4,3/4,1,2,3,4$ (measured in soliton periods) to illustrate the main pulse shaping mechanisms in Figs. 5 and 6 for the Kerr and Raman models, respectively. Only the field intensity envelopes are shown, but the corresponding spectra were obtained from the full complex E field. After four soliton periods the most intense part of the pulse has separated from the two other constituents by a small amount approximately equal to $1.5ct_0$ in Fig. 5. The intensities are in agreement with results from the IST, $(5/3)^2,1,(1/3)^2$. The weaker leading soliton is not visible on the scale of the graph. In Fig. 6 the soliton self-frequency shift is evidenced by the appearance of two Stokes bands. After a quarter soliton period the pulse reaches its maximal compression (the foci point; see Fig. 3) and spectral asymmetry is already visible (compare to Fig. 5), with a dominant peak near $(k-k_0)ct_0\sim n_0\Omega_v t_0\sim 1.23$ (447 cm^{-1}). The Stokes wing is clearly enhanced due to Raman pumping from higher frequencies. RSS therefore destroys the periodic breathing pattern of higher-order bright solitons. The soliton decays into fragments after only three-

quarters of a soliton period, which rapidly separate from each other (compare with previous figures).

The shortest and most intense fragment shapes after a few periods to form a fundamental soliton (see Fig. 3) whose subsequent evolution is governed by dispersion, self-phase modulation, and Raman self-frequency shift. Numerical simulations indicated that the fragments evolve without frequency chirp, in contrast to the case $\theta=0$, where a small negative frequency chirp at the leading edge and a positive chirp at the trailing side were observed due to the joint action of GVD and self-phase modulation.

IV. CONCLUSIONS

In conclusion, using the FD TD method, recently applied to the field of nonlinear optics [19], we have illustrated the fragmentation of higher-order bright solitons from Maxwell's equation in a nonlinear Lorentz medium characterized by chromatic anomalous dispersion and nonlinear dispersion. A comparison with an instantaneous nonlinearity indicated that even in the absence of Raman self-scattering, higher-order solitons decay into their constitutive components due to the higher-order dispersive effects (third-order dispersion and self-steepening). The dynamics of the soliton pulse width, intensity, and spatial and spectral profile evidenced the formation of the fundamental soliton from the rest of the multisoliton pulse. Oscillations in the pulse width and intensity are understood as a result of the interference of the forming main Stokes soliton with the rest of the pulse. Only the short intense Stokes pulse will experience a considerable frequency shift since the efficiency of Raman scattering depends on the pulse intensity and width. Raman self-scattering can therefore be regarded as a nonlinear filter for short intense optical pulses.

ACKNOWLEDGMENTS

L.G. is grateful to the Ministerio de Educación y Cultura of Spain for a research grant. L.V. is thankful for partial support from the Comisión Interministerial de Ciencia y Technología of Spain (Grant No. PB95-0426). L.G. wishes to thank the optics group of Imperial College, London, where part of this work was carried out.

[1] G.P. Agrawal, *Nonlinear Fiber Optics*, 2nd ed. (Academic, New York, 1995); V. Konotop and L. Vázquez, *Nonlinear Random Waves* (World Scientific, Singapore, 1994).
[2] T. Taniuti, Prog. Theor. Phys. Suppl. **55**, 1 (1974).
[3] J.R. Taylor, *Optical Solitons, Theory and Experiment* (Cambridge University Press, Cambridge, 1992).
[4] R.R. Alfano, *The Supercontinuum Laser Source* (Springer-Verlag, Berlin, 1989).
[5] A. Baltuska *et al.*, Opt. Lett. **22**, 102 (1997).
[6] J.P. Gordon, Opt. Lett. **11**, 662 (1986).
[7] F.M. Mitschke and L.F. Mollenauer, Opt. Lett. **11**, 659 (1986).
[8] W. Hodel and H.P. Weber, Opt. Lett. **12**, 924 (1987); P. Beaud, W. Hodel, B. Zysset, and H.P. Weber, IEEE J. Quantum Electron. **QE-23**, 1938 (1987); Y. Kodama and K. Nozaki, Opt. Lett. **12**, 1038 (1987); K. Tai, A. Hasegawa, and N. Bekki, *ibid.* **13**, 392 (1988); K.J. Blow and D. Wood, IEEE J. Quantum Electron. **QE-25**, 2665 (1989); P.V. Mamyshev and S.V. Chernikov, Opt. Lett. **15**, 1076 (1990); R.H. Stolen and W.J. Tomlinson, J. Opt. Soc. Am. B **9**, 565 (1992).
[9] B. Zysset, P. Beaud, and W. Hodel, Appl. Phys. Lett. **50**, 1027 (1987); P. Beaud, W. Hodel, B. Zysset, and H.P. Weber, IEEE J. Quantum Electron. **QE-23**, 1938 (1987); A.S. Gouveia-Neto, A.S.L. Gomes, and J.R. Taylor, *ibid.* **QE-24**, 332 (1988); S.V. Chernikov and P.V. Mamyshev, J. Opt. Soc. Am. B **8**, 1633 (1991).
[10] G.P. Agrawal and C. Headley III, Phys. Rev. A **46**, 1573 (1992); Y.S. Kivshar and B.A. Malomed, Opt. Lett. **18**, 485 (1993).
[11] R. G. Flesch, A. Pushkarev, and J. V. Moloney, Phys. Rev. Lett. **76**, 2488 (1996).
[12] S.L. Liu and W.Z. Wang, Opt. Lett. **18**, 1911 (1993).
[13] C.G. Goedde, W.L. Kath, and P. Kumar, Opt. Lett. **19**, 2077 (1994); J. Opt. Soc. Am. B **14**, 1371 (1997).
[14] F.M. Mitschke and L.F. Mollenauer, Opt. Lett. **12**, 355 (1987).
[15] E.L. Buckland, R.W. Boyd, and A.F. Evans, Opt. Lett. **22**, 454 (1997).
[16] Y. Kodama and A. Hasegawa, IEEE J. Quantum Electron. **QE-23**, 510 (1987).
[17] K.J. Blow and D. Wood, IEEE J. Quantum Electron. **25**, 2665 (1989); P.V. Mamyshev and S.V. Chernikov, Opt. Lett. **15**, 1076 (1990).
[18] T. Brabec and F. Krausz, Phys. Rev. Lett. **78**, 3282 (1997).
[19] R.M. Joseph and A. Taflove, IEEE Trans. Antennas Propag. **45**, 364 (1997); A. Taflove, *Computational Electrodynamics: The Finite-Difference Time-Domain Method* (Artech, Norwood, 1995); P.M. Goorjian and A. Taflove, IEEE J. Quantum Electron. **28**, 2416 (1992).
[20] P.N. Butcher and D. Cotter, *The Elements of Nonlinear Optics* (Cambridge University Press, Cambridge, 1990).
[21] R.W. Hellwarth, A. Owyoung, and N. George, Phys. Rev. A **4**, 2342 (1971).
[22] A.C. Newell and J.V. Moloney, *Nonlinear Optics* (Addison-Wesley, Reading, MA, 1992); E.G. Sauter, *Nonlinear Optics* (Wiley, New York, 1996).
[23] Y.R. Shen, *The Principles of Nonlinear Optics* (Wiley, New York, 1984).
[24] R.H. Stolen, J.P. Gordon, W.J. Tomlinson, and H.A. Hauss, J. Opt. Soc. Am. B **6**, 1159 (1989).
[25] P.G. Petropoulos, IEEE Trans. Antennas Propag. **42**, 62 (1994); **42**, 859 (1994).
[26] H. Bachiri, L. Gilles, and L. Vázquez (unpublished); Guo Ben-Yu, I. Martín, V. M. Pérez García, and L. Vázquez, J. Comput. Phys. **129**, 181 (1996).
[27] V.E. Zakharov and A.B. Shabat, Sov. Phys. JETP **34**, 62 (1972); J. Satsuma and N. Yajima, Prog. Theor. Phys. Suppl. **55**, 284 (1974).